Journal of Sound and Vibration (1997) **208**(2), 189–209

AN INVESTIGATION OF THE SELF-LOOSENING BEHAVIOR OF BOLTS UNDER TRANSVERSE VIBRATION

R. I. ZADOKS

Mechanical and Industrial Engineering Department, The University of Texas at El Paso, El Paso, Texas 79968, *U.S.A.*

AND

X. YU

New Venture Gears, East Syracuse, New York 13057, *U.S.A.*

(*Received* 19 *August* 1996, *and in final form* 28 *May* 1997)

Although a great deal of research has focused on the reliability of bolts, self-loosening, which is a main cause of failure of bolted connections, is still not fully understood. To develop a complete model of the self-loosening behavior of a transversely excited bolted connection, an extensive study of the mechanisms of bolt self-loosening is presented here. In this work, the theory of Hertz contact stress is employed to find a contact stiffness. Using this stiffness with a two-degree-of-freedom dynamic model gives the transverse force applied to the bolt when the bolted connection is subjected to dynamic excitation. This transverse force is found to be an important factor in self-loosening. Based on the results from static and dynamic models, a main cause of bolt self-loosening is found to be impacting between the clamped mass and the clamping bolt, and the process of bolt self-loosening is predicted. This prediction can be favorably compared to experimental results.

1. INTRODUCTION

Approximately 200 billion fasteners are produced annually in the United States and there is a growing demand for more reliable threaded fasteners [1]. After fatigue, self-loosening is the most frequent cause of failure of dynamically loaded bolted connections. Additionally, fatigue is often initiated by partial loosening. Despite the importance of self-loosening in bolted connections, complete physical and mathematical models of the underlying physical phenomena do not currently exist in the literature.

Goodier and Sweeney [2] and Sauer *et al*. [3] tested bolted connections that were dynamically loaded in the axial direction (parallel to the bolt axis). In spite of their failures to obtain a complete model for the self-loosening of the threaded fasteners, they offered an explanation for self-loosening that does contain the primary mechanism. In these models bolted connections loosened due to the relative motion between the thread flanks and other contact surfaces of the clamped and clamping parts.

In 1969, Junker [4] presented the most important paper on threaded fastener loosening to date. In this work Junker described experiments that were run with a new kind of machine (now called the "Junker machine"). With this apparatus, Junker obtained relationships among the relative displacement between clamped parts, a transverse force (perpendicular to the bolt axis), and the axial preload applied to the bolt.

0022–460X/97/470189 + 21 $25.00/0/sv971173

Sakai [5] investigated loosening mechanisms for a bolt at the center of rotation of a pair of clamped parts while these parts were twisted. He also investigated the effect of transverse loads on the bolt and drew the conclusion that the necessary condition for a bolt to loosen is that the friction coefficient at the threads must be less than 0·03. However, when unlubricated metal-to-metal contact occurs, the friction coefficient is much greater than 0·03. Obviously, other casuses of self-loosening must exist.

Koga and Isono [6, 7] studied the behavior of bolts, including the characteristics of impulsive friction. They suggested the following theory concerning the causes of dynamic bolt loosening. When a bolt is subjected to axial impacts, the stress waves inside the bolt body cause the axial preload (clamping force) to decrease, and then the bolt loosens. However, this hypothesis contradicts the experimental results presented by other researchers, which show that axial vibrations seldom cause bolt loosening [4, 5].

In a recent paper [8], Hess presents analytical and experimental results for the loosening and tightening of a sinlge threaded fastener which is subject to axial vibrations. In this paper, loosening occurs when the resultant of the frictional moments, which are functions of the dynamic motion, becomes smaller than the moment, acting in the loosening direction, from the normal thread contact force. This self-loosening mechanism is similar to the mechanism presented in this paper for transversely vibrated bolted connections. However, the effects that lead to variations in the frictional moments are quite different between the axially excited and transversely excited cases.

As can be seen, the existing literature has been limited to investigations of only certain aspects of bolt self-loosening. To develop a complete model of this phenomenon, an extensive study of the mechanisms of bolt self-loosening, including static and dynamic behavior, is necessary. In this paper, a mathematical model of a bolted connection is investigated to determine the real causes of self-loosening when the connection is subjected to transverse excitation. This analysis reveals that impacts between the clamped parts and the bolt are necessary conditions for dynamic loosening. To determine the amplitude and duration of the impact force, a two-degree-of-freedom dynamic model with a non-continuous stiffness is established, in which Hertz contact stress theory is adopted to obtain an equivalent contact stiffness. To evaluate the complete motion of the bolted connection, a variable time step computational approach is used. With this simulation the number of impacts, and their durations and amplitudes, can be predicted. Combining these results with the critical transverse force obtained previously [9, 10] leads to the prediction of the self-loosening process. All of these results are validated experimentally.

2. HERTZ CONTACT FORCE AND CONTACT STIFFNESS IN IMPACT

A simple model for a single bolted connection is selected (see Figure 1). A mass (circular disk) is fastened to a large plate by a bolt which passes through a circular hole in the mass. This bolt applies a preload Q to the mass. The system is excited by a transverse

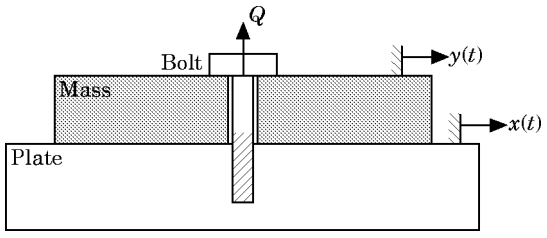

Figure 1. Model of a transversely excited bolted connection.

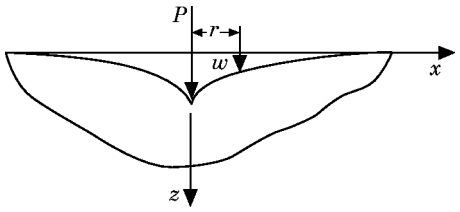

Figure 2. Displacement w due to force P on an elastic plane.

displacement $x(t)$ which is applied to the plate. If the amplitude and frequency of this displacement are increased to some levels, then the mass will move relative to the plate. Larger relative displacements may lead to impacting between the mass and the bolt. As will be seen, the amplitude and duration of the impact forces are significant factors in the self-loosening of bolts. To determine the amplitude and duration of these impact forces, Hertz contact theory is first used to derive a relationship between the deformations of the mass and bolt, and the contact force during the impact.

This derivation begins by considering an elastic plane (Figure 2). A concentrated force P applied to the plane causes a displacement w at another point away from P; w is given by [11]

$$w = P(1 - v^2)/\pi Er, \tag{1}$$

r is the distance between P and the point with displacement w. E is Young's modulus and v is Poisson's ratio for the material of the elastic plane.

When two cylinders with different radii are in contact, the intensity of the pressure p over the surface of contact is reasonably represented by the ordinates of a semi-ellipsoid constructed on the surface of contact [11]. The lengths of the semiaxes of the ellipse are b and p_0 (see Figure 3). The maximum pressure value clearly exists at the center of the surface of contact. The equation of the ellipse is

$$p^2/p_0^2 + x^2/b^2 = 1. \tag{2}$$

The total contact force F is obtained by integrating the pressure p over the entire contact area:

$$F = \int_A (p)\, \mathrm{d}A = \pi abp_0. \tag{3}$$

Under the application of the contact force F, the bolt and mass of Figure 1 have displacements w_1 and w_2, respectively. Let

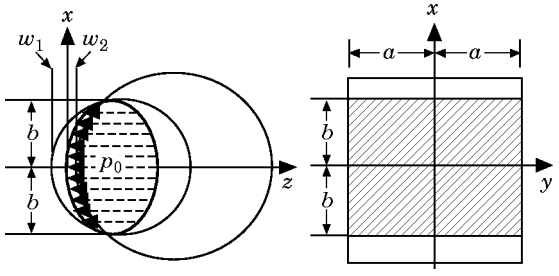

Figure 3. Stress distribution over the contact area between the bolt shank and the mass.

$$u = w_1 + w_2, \tag{4}$$

where u represents an amount of interpenetration between the bolt and mass. Using equation (1), u is given by

$$u = w_1 + w_2 = \left[\frac{(1 - v_b^2)}{\pi E_b} + \frac{(1 - v_d^2)}{\pi E_d}\right] \int_A \left(\frac{p}{r}\right) \mathrm{d}A$$

$$= [k_b + k_d] p_0 \int_{-a}^{a} \left[\int_{-b}^{b} \sqrt{\frac{1 - x^2/b^2}{x^2 + y^2}}\, \mathrm{d}x\right] \mathrm{d}y, \tag{5}$$

where E_b and v_b, and E_d and v_d are Young's modulus and Poisson's ratio, respectively, for the bolt and the mass, respectively, and

$$k_b = (1 - v_b^2)/\pi E_b, \qquad k_d = (1 - v_d^2)/\pi E_d. \tag{6}$$

Noting the symmetry of the limits of integration and of the integrand, equation (5) reduces to

$$u(b) = 4[k_b + k_d] \int_0^a \left[\int_0^b \sqrt{\frac{1 - x^2/b^2}{x^2 + y^2}}\, \mathrm{d}x\right] \mathrm{d}y$$

$$= 4[k_b + k_d] p_0 \int_0^b \sqrt{1 - \frac{x^2}{b^2}} \log \frac{a + \sqrt{x^2 + a^2}}{x}\, \mathrm{d}x. \tag{7}$$

This elliptic integral is difficult to evaluate in closed form and, therefore, numerical integration is adopted to obtain the function $u(b)$. Since the integrand goes to infinity as x approaches zero, the integral in equation (7) is improper. The convergence of this integral must be established before numerical integration can be used to evaluate equation (7).

The limit test [12] can be used to establish the convergence of the integral in equation (7). The integral $I(a, b)$,

$$I(a, b) = \int_a^b f(x)\, \mathrm{d}x, \tag{8}$$

is improper because, while $f(x)$ is a continuous function $f(x) \geqslant 0$ in $[a, b]$,

$$\lim_{x \to a} f(x) = \infty. \tag{9}$$

It can be shown that $I(a, b)$ will converge if for a constant q, $0 < q < 1$, the limit exists:

$$\lim_{x \to a} (x - a)^q f(x). \tag{10}$$

Based on this theorem and using l'Hôpital's rule [12]:

$$\lim_{x \to a} (x - a)^q \sqrt{1 - x^2/b^2} \log ([a + \sqrt{x^2 + a^2}]/x) = 0 \quad \text{for} \quad 0 < q < 1. \tag{11}$$

Therefore, the integral in equation (7) converges. Given a constant $0 < \varepsilon \ll 1$, $u(b)$ in equation (7) is approximated by [13]

$$u(b) \approx 4[k_b + k_d]\, p_0 \int_{0+\varepsilon}^{b} \sqrt{1 - x^2/b^2} \log ([a + \sqrt{x^2 + a^2}]/x)\, \mathrm{d}x. \tag{12}$$

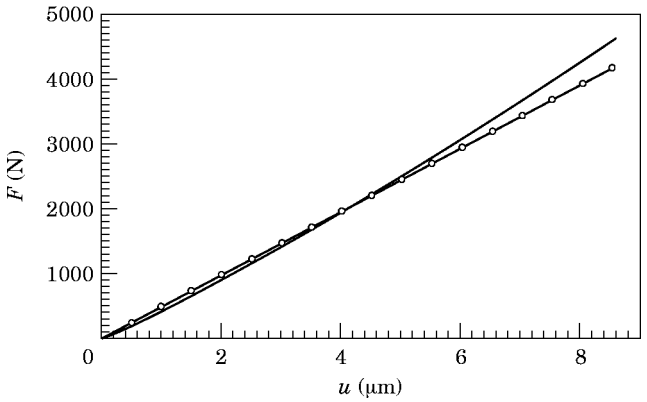

Figure 4. Relationship between the contact force F and relative displacement u_1: ——, calculated data; –○–, linear approximation.

The integration in equation (12) can be implemented numerically.

The integral in equation (12) is a function of b known as $\gamma(b)$. Therefore,

$$u(b) = 4(k_b + k_d)p_0\,\gamma(b). \tag{13}$$

From equation (3), p_0 is given by

$$p_0 = F/(\pi ab). \tag{14}$$

Substituting equation (14) into equation (13) yields

$$u = \left(\frac{4(k_b + k_d)}{\pi ab}\right)F\gamma(b). \tag{15}$$

Timoshenko [11] has derived a relation for b as a function of F:

$$b = \sqrt{4F(k_b + k_d)R_1\,R_2\,/(R_1 + R_2)}, \tag{16}$$

where R_1 takes the negative value of the radius of the hole in the mass, and R_2 takes the positive value of the radius of the bolt. For a given value F, equation (16) provides a value for b. Then $\gamma(b)$ is obtained by numerically integrating the integral of equation (12). Substituting values for b and $\gamma(b)$ into equation (15) yields a relationship between u and F, as shown in Figure 4. This relationship is seen to be almost linear, and it can be approximated as

$$F = k_1\,u, \tag{17}$$

where the constant k_1 is the contact stiffness. The values used to produce the results presented in Figure 4 are listed in Table 1.

3. IMPACT FORCE AND IMPACT DURATION

When an impact occurs, the bolt bends due to the impact force. The bending stiffness of the bolt then affects the amplitude and duration of the impact. Therefore the system composed of the bolt and the mass may be modeled as a mass–spring system, combining the effects of Hertz contact and bending (see Figure 5). In Figure 5, m_b and m_d are the masses of the bolt and mass, respectively, c_1 and c_2 are damping coefficients of the bolt in Hertz contact and in bending, respectively, k_1 is the Hertz contact stiffness, and k_2 is

TABLE 1

Values used to determine the Hertz contact stiffness k_1

Symbol	Definition	Value
R_1	Radius of hole in mass (mm)	−3·2169
R_2	Radius of bold shank (mm)	+3·1750
E_b	Young's modulus for bolt (GPa)	200·0
E_d	Young's modulus for mass (GPa)	200·0
v_b	Poisson's ratio for bolt	0·300
v_d	Poisson's ratio for mass	0·300
For impact simulation (Figure 8)		
a	Height of contact area (mm)	6·35
k_1	Hertz contact stiffness (N/m)	4·90 E8
For self-loosening simulations (Figures 16 and 17)		
a	Height of contact area (mm)	13·97
k_1	Hertz contact stiffness (N/m)	9·28 E8

the bending stiffness of the bolt. $x_1(t)$ and $y(t)$ are the absolute displacements of the bolt shank and the mass, respectively. $x(t)$ is the excitation displacement of the plate:

$$x(t) = -A_d \cos \Omega(t + t_0), \tag{18}$$

where A_d is the amplitude of the excitation, Ω is the frequency of the excitation, and t_0 is a time delay that accounts for the time of the onset of an impact. f_{f1} and f_{f2} represent the friction forces between the mass and the plate (interface 1) and between the mass and the bolt head (interface 2), respectively:

$$f_{f1} = \mu_1 (Q + m_d g) \operatorname{sgn}(\dot{y} - \dot{x}), \qquad f_{f2} = \mu_2 Q \operatorname{sgn}(\dot{y} - \dot{x}_1). \tag{19}$$

Hunt and Crossley [14] presented a model of the Hertz contact forces, including damping:

$$F = k_1 u^n (1 + \lambda \dot{u}^q), \tag{20}$$

where u and $\dot{u}$ are the relative displacement and velocity between the contacting surfaces, respectively, n is a value that depends on the geometries of the surfaces in contact ($n = 1$ for two flat plates in contact and 1·5 for a sphere impacting a plate), k_1 and λ depend on the material properties and geometries of the bodies in contact, and q is an arbitrary integer value (results are presented in reference [14] for $q = 1$ and 2). Taking n and q both equal to unity, the contact force of equation (20) becomes

$$F = k_1 u + c_1 u\dot{u}, \tag{21}$$

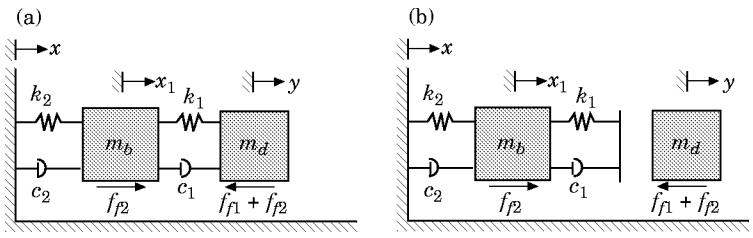

Figure 5. Dynamic model of the bolted connection: (a) during contact; (b) without contact.

which includes the non-linear dissipative term $c_1 u\dot{u}$. However, to simplify the simulation process described in section 7 below, it is desired to have piecewise linear equations of motion. Therefore, it is assumed here that the Hertz contact force has the form

$$F = k_1 u + c_1 \dot{u}. \tag{22}$$

The affects of this assumption will be discussed in section 8.

The governing differential equations of motion are then found to be (after reference [16]):

$$\begin{aligned} m_b \ddot{x}_1 + c_2 \dot{x}_1 + k_2 x_1 - \{c_1 (\dot{y} - \dot{x}_1) + k_1 [y - x_1 - (E/2)\mathrm{sgn}\,(y - x_1)]\}\delta \\ = c_2 \dot{x} + k_2 x + f_{f2}, \\ m_d \ddot{y} + \{c_1 (\dot{y} - \dot{x}_1) + k_1 [y - x_1 - (E/2)\,\mathrm{sgn}\,(y - x_1)]\}\delta = -f_{f1} - f_{f2}, \end{aligned} \tag{23}$$

where δ is a Kroenecker delta function used to model the transition from the system of Figure 5(a) to the system of Figure 5(b), and back:

$$\delta = \begin{cases} 1, & \text{if} \quad |y - x_1| \geqslant E/2, \\ 0, & \text{if} \quad |y - x_1| < E/2. \end{cases} \tag{24}$$

In actuality it is more convenient to examine equations (23) in terms of two relative displacements:

$$z \equiv y - x, \qquad z_1 \equiv y - x_1, \tag{25, 26}$$

where z represents the relative displacement of the mass with respect to the plate, and z_1 represents the relative displacement between the mass and the bolt. Substituting equations (25) and (26) into equations (23), (19) and (24), respectively, yields

$$m_b (\ddot{z} - \ddot{z}_1) + c_2 (\dot{z} - \dot{z}_1) + k_2 (z - z_1) - \{c_1 \dot{z}_1 + k_1 z_1\}\delta = -m_b \ddot{x} - k_1 (E/2)\,\mathrm{sgn}\,(z_1)\delta + f_{f2},$$

$$m_d \ddot{z} + \{c_1 \dot{z}_1 + k_1 z_1\}\delta = -m_d \ddot{x} + k_1 (E/2)\,\mathrm{sgn}\,(z_1)\delta - f_{f1} - f_{f2}, \tag{27}$$

$$f_{f1} = \mu_1 (Q + m_d g)\,\mathrm{sgn}\,(\dot{z}), \qquad f_{f2} = \mu_2 Q\,\mathrm{sgn}\,(\dot{z}_1), \tag{28}$$

$$\delta = \begin{cases} 1, & \text{if} \quad |z_1| \geqslant E/2, \\ 0, & \text{if} \quad |z_1| \geqslant E/2. \end{cases} \tag{29}$$

It should be noted that the friction coefficients μ_1 and μ_2 will be represented in the simulations presented below in terms of static (μ_{s1} and μ_{s2}, respectively) and kinetic (μ_{k1} and μ_{k2}, respectively) values. When $\dot{z}$ or $\dot{z}_1$ is equal to zero, the respective friction force is determined by assuring equilibrium at the corresponding interface. Motion resumes when this friction force exceeds the value of the corresponding static friction force as determined by equation (28) using the static friction coefficient μ_{s1} or μ_{s2}.

There are seven different states of motion that must be considered, based on the three sgn functions that appear in equations (27):

(1) slip at interface 1, slip at interface 2, contact between mass and bolt;
(2) slip at interface 1, slip at interface 2, no contact between mass and bolt;
(3) stick at interface 1, slip at interface 2, contact between mass and bolt;
(4) stick at interface 1, slip at interface 2, no contact between mass and bolt;
(5) slip at interface 1, stick at interface 2, contact between mass and bolt;
(6) slip at interface 1, stick at interface 2, no contact between mass and bolt;
(7) stick at interface 1, stick at interface 2.

TABLE 2

Possible motion state transitions

From	To	Criteria	From	To	Criteria
1	2	$\|z_1\| \to E/2$	2	1	$\|z_1\| \to E/2$
1	3	$\|\dot{z}\| \to 0$	2	4	$\|\dot{z}\| \to 0$
1	5	$\|\dot{z}_1\| \to 0$	2	6	$\|\dot{z}_1\| \to 0$
3	1	$\|f_{f1}\| \to \mu_{s1}(Q + m_d g)$†	4	2	$\|f_{f1}\| \to \mu_{s1}(Q + m_d g)$†
3	4	$\|z_1\| \to E/2$	4	3	$\|z_1\| \to E/2$
3	7	$\|\dot{z}_1\| \to 0$	4	7	$\|\dot{z}_1\| \to 0$
5	1	$\|f_{f2}\| \to \mu_{s2} Q$‡	6	2	$\|f_{f2}\| \to \mu_{s2} Q$‡
5	7	$\|\dot{z}\| \to 0$	6	7	$\|\dot{z}\| \to 0$
7	3 or 4	$\|f_{f2}\| \to \mu_{s2} Q$§			
7	5 or 6	$\|f_{f1}\| \to \mu_{s1}(Q + m_d g)$‖			

† $f_{f1} = -\{m_d \ddot{x} + (k_1[z_1 - (E/2)\ \mathrm{sgn}\ (z_1)] + c_1 \dot{z}_1)\delta + \mu_{k2} Q\ \mathrm{sgn}\ (\dot{z}_1)\}$

‡ $f_{f2} = (m_d/[m_d + m_b])[k_2(z - z_1) + c_2 \dot{z}] - k_1[z_1 - (E/2)\ \mathrm{sgn}\ (z_1)]\delta$
$-(m_b/[m_d + m_b])\mu_{k1}(Q + m_d g)\ \mathrm{sgn}\ (\dot{z})$

§ $f_{f2} = m_b \ddot{x} + k_2(z - z_1) - k_1[z_1 - (E/2)\ \mathrm{sgn}(z_1)]\delta$

‖ $f_{f1} = -\{(m_d + m_b)\ddot{x} + k_2(z - z_1)\}$

While these states could be considered simultaneously using the formulation in equations (27), it is more convenient from a computational outlook to consider them separately. Additionally, it is imperative to determine the transitions between states precisely. Table 2 shows the possible transitions from the seven states listed above.

To find z_1 and the impact force F, one still needs the values of four parameters, k_1, k_2, c_1 and c_2, as shown in Figure 5. The value of k_1 for this situation was determined using Figure 4 (see Table 1). k_2 is the bending stiffness of the bolt. During the experiments that were conducted to verify the impact force and duration (see Figure 6 and Figure 7), the bolt was tightly threaded against the shaker table (below the plate) so that no relative displacements between the bolt and the shaker table could take place. Therefore, it can reasonably be assumed that the bolt acted as a cantilevered beam with a fixed end, and the bending stiffness k_2 can be found by using Timoshenko beam theory [15]:

$$k_2 = 12E_b I/[L_3^2 (L_3 + 3L_4)], \tag{30}$$

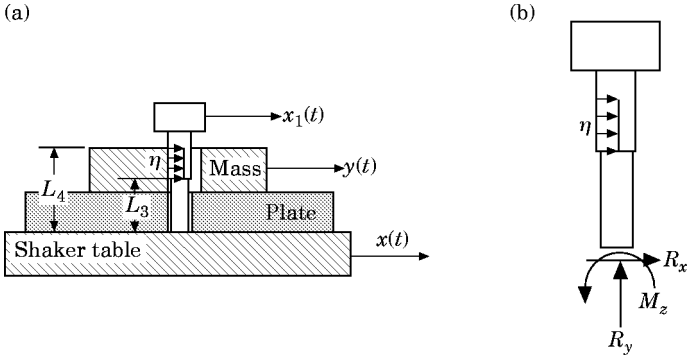

Figure 6. (a) Cantilevered Timoshenko beam model of the bolt for the impact test, (b) the free body diagram of the bolt.

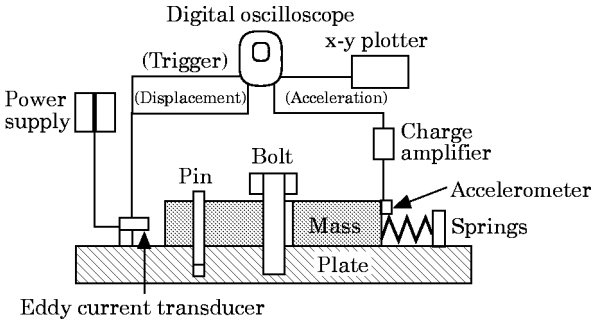

Figure 7. Experimental setup for impact force measurements.

where L_3 is the length of the bolt from its threaded end to the bottom of the unthreaded shank (see Figure 6), L_4 is the length of the bolt from its threaded end to the top of the mass, and I is the moment of area of the bolt cross-section:

$$I = \pi R_2^4 / 4. \tag{31}$$

The values for the system studied in this paper are listed in Table 3.

The values of c_1 and c_2 are determined indirectly, by assuming stiffness proportional damping:

$$[\mathbf{C}] = \begin{bmatrix} c_1 + c_2 & -c_1 \\ -c_1 & c_1 \end{bmatrix} = \beta \begin{bmatrix} k_1 + k_2 & -k_1 \\ -k_1 & k_1 \end{bmatrix}. \tag{32}$$

If the equations of motion are uncoupled using the normalized modal matrix [**P**] for the undamped, homogeneous form of equations (23), then the damping coefficient matrix [**C**] of equation (32) is transformed into the diagonal form:

$$[\mathbf{P}]^{\mathrm{T}} [\mathbf{C}] [\mathbf{P}] = \begin{bmatrix} 2\zeta_1 \omega_1 & 0 \\ 0 & 2\zeta_2 \omega_2 \end{bmatrix} = \begin{bmatrix} \beta\omega_1^2 & 0 \\ 0 & \beta\omega_2^2 \end{bmatrix}. \tag{33}$$

TABLE 3

Values used in the impact simulation

Symbol	Definition	Value
E_b	Young's modulus for bolt (GPa)	200·0
L_3	Length of threaded section of bolt (mm)	13·331
L_4	Active length of bolt (mm)	17·4625
R_2	Radius of bolt shank (mm)	3·175
k_2	Bending stiffness of bolt (N/m)	1·64E7
ζ_1	First modal damping factor	0·001
β	Damping to stiffness constant ratio (s)	8·926E-7
D	Diameter of sliding mass (mm)	203·0
d	Diameter of slot in sliding mass (mm)	6·4338
h	Thickness of sliding mass (mm)	12·7
ρ	Density of sliding mass (kg/m^3)	7840·0
m_d	Mass of sliding mass (kg)	3·151
$\dot{z}_1(0)$	Initial velocity of sliding mass (m/s)	0·656

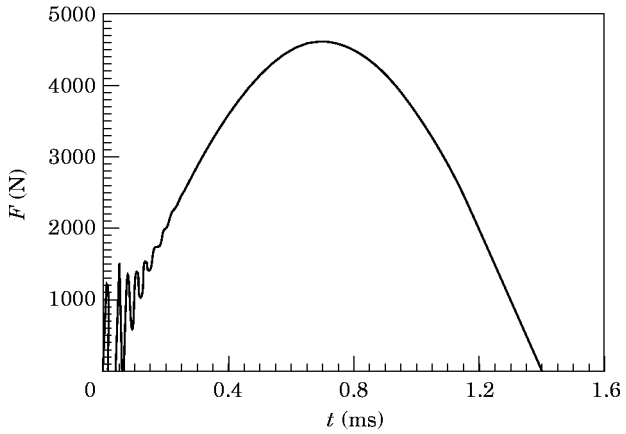

Figure 8. Simulation of the impact force between the bolt and the mass.

Then, β can be selected to give the desired value of either of the modal damping factors, ζ_1 and ζ_2 (see Table 3).

Now, the time history of the impact force F can be obtained. Previously it was shown that the impact force F is proportional to the relative displacement z_1 when $z_1 > 0$ (see Figure 4), while the force vanishes for $z_1 \leqslant 0$, i.e.,

$$F = \begin{cases} k_1 z_1, & z_1 > 0, \\ 0, & z_1 \leqslant 0. \end{cases} \tag{34}$$

Figure 8 shows the impact force F calculated using the model of equations (27).

4. VERIFICATION OF THE IMPACT FORCE

Experiments were run to verify the mathematical model of the impact force that was derived in the previous section. The layout of the experimental apparatus is shown in Figure 7. A plate is firmly attached to a shaker table. Then a mass is placed on the plate, and a bolt is passed through an untapped slot in the mass and threaded into a tapped hole in the plate. The length of the bolt is selected so that it bottoms out on the shaker table without applying a preload to the mass. Dimensions of the mass are listed in Table 3.

At the beginning of the test, the mass was held by a straight pin, inserted through the mass and into the plate, despite being pushed by two compression springs. Once the pin was pulled out, the springs pushed the mass across the plate until the mass collided with the bolt. An eddy current transducer mounted on the plate measured the displacement of the mass as a function of time. This information indirectly provided the velocity of the mass as it slid. An accelerometer mounted on the mass was used to measure the acceleration of the mass. Both the displacement and the acceleration signals were amplified, and these amplified signals were captured by a digital oscilloscope which was triggered by the displacement signal from the eddy current transducer. An X–Y plotter was used to record the results permanently.

The experiment was repeated over 100 times. Since the velocity immediately before impact depends on the initial conditions at the release of the mass (removal of the pin), it was found to be difficult to duplicate exactly the results of this experiment. However, as long as the impact velocities were the same between two trials, the measured

accelerations of the mass were also identical. The impact velocity $\dot{z}_1(0)$ for this example is given in Table 3.

The impact force as predicted by the model of Figure 5 and Figure 6 is shown in Figure 8. This force mainly consists of a low frequency (356 Hz) component and a high frequency (35·9 kHz) component. The calibration of the measurement system showed that the component with the higher frequency (35·9 kHz) could not be measured. Therefore, a low pass filter was applied to the analytical results so that these results could be compared directly to the experimental values. Figure 9 shows this comparison and it is seen that the predicted results agree quite favorably with the experimental results. It should be noted that the values of k_2 and $\dot{z}_1(0)$ were adjusted slightly from their original theoretical values to produce this result. The values used to produce Figure 9 are listed in Table 3.

5. CIRCUMFERENTIAL FRICTION FORCES OPPOSING LOOSENING

The basic physical phenomenon that plays the pivotal role in the self-loosening mechanism of transversely excited bolted connections is Coulomb friction. It is the friction between the male and female threads that allows a bolted connection to stay tight despite an off-torque that tends to loosen the connection. This off-torque is due to the axial force in the bolt and the fact that the threads are helical inclined planes [5]. Since no additional torques are applied to the bolt during self-loosening, something must occur to reduce the effect of friction on the threads.

To begin this discussion, imagine a block on a table (see Figure 10). The block can be moved in direction 1 by the application of a force (force 1). Assuming the action of Coulomb friction between the block and the table, the value of the force required to cause motion is infinitesimally larger than the value of the frictional force between the block and the table. If another force (force 2) is applied to the block in direction 2, then the block will move with a component in direction 2 with an acceleration equal to force 2 divided by the mass of the block. That is, at the instant that force 2 is applied, the force of friction is zero in the direction which is perpendicular (i.e., direction 2) to the direction of motion (i.e., direction 1) [4, 17].

Once the block starts moving in direction 3, for example, under the application of force 1 and force 2, the value of the frictional force in direction 2 is no longer zero. This is

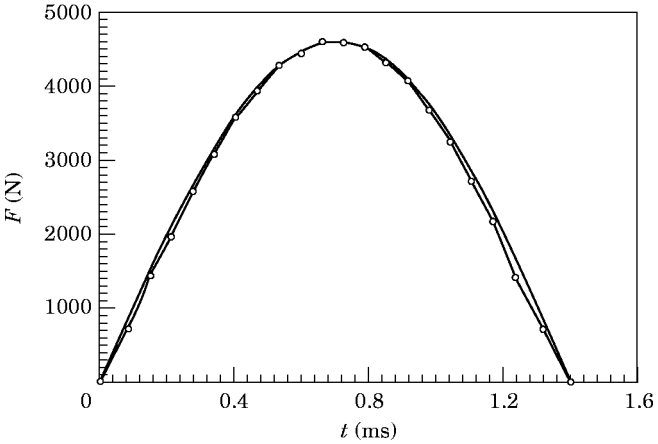

Figure 9. Comparison of the simulated and experimental impact forces: ——, simulation result; —○—, experimental data.

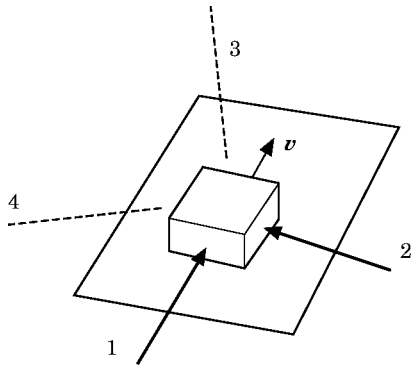

Figure 10. A block sliding on a plane subject to a force perpendicular to the direction of motion.

because the velocity of the block now has a component in direction 2. Instead, the friction force is zero in direction 4, which is perpendicular to direction 3. Therefore, any force applied in direction 4 leads to an acceleration that is proportional to the force in this direction. This process continues for any new direction of motion.

Now, consider the situation shown in Figure 11, which represents the contact area on a thread or at the bolt head. $\mathbf{v}_t$ is the relative transverse velocity between the male and female thread forms or between the bolt head and the clamped part. $\mathbf{v}_c$ is the relative circumferential velocity that occurs when the total friction torque is smaller than the off-torque. The resultant relative velocity $\mathbf{v}$ is given by

$$\begin{aligned}\mathbf{v} &= (|\mathbf{v}_t| + |\mathbf{v}_c| \cos(\pi/2 + \theta))\mathbf{i} + |\mathbf{v}_c| \sin(\pi/2 + \theta)\mathbf{j} \\ &= (|\mathbf{v}_t| - |\mathbf{v}_c| \sin\theta)\mathbf{i} + |\mathbf{v}_c| \cos\theta\mathbf{j}. \end{aligned} \tag{35}$$

α is the angle between $\mathbf{v}_c$ and $\mathbf{v}$, where:

$$\begin{aligned}\cos\alpha = \frac{\mathbf{v}\cdot\mathbf{v}_c}{|\mathbf{v}||\mathbf{v}_c|} &= \frac{[(|\mathbf{v}_t| - |\mathbf{v}_c| \sin\theta)\mathbf{i} + |\mathbf{v}_c| \cos\theta\mathbf{j}] \cdot [-|\mathbf{v}_c| \sin\theta\mathbf{i} + |\mathbf{v}_c| \cos\theta\mathbf{j}]}{|\mathbf{v}_c| \sqrt{(|\mathbf{v}_t| - |\mathbf{v}_c| \sin\theta)^2 + (|\mathbf{v}_c| \cos\theta)^2}} \\ &= (|\mathbf{v}_c| - |\mathbf{v}_t| \sin\theta)/\sqrt{|\mathbf{v}_t|^2 - 2|\mathbf{v}_t||\mathbf{v}_c| \sin\theta + |\mathbf{v}_c|^2}. \end{aligned} \tag{36}$$

The velocity ratio Λ is then defined as

$$\Lambda = \frac{|\mathbf{v}_c|}{|\mathbf{v}_t|}. \tag{37}$$

Substituting equation (37) into equation (36) yields

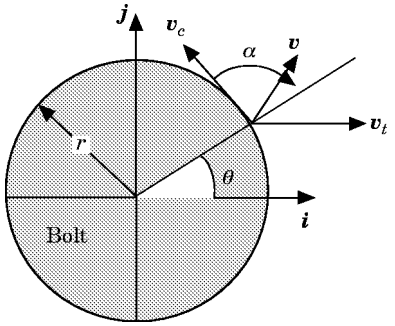

Figure 11. Total relative velocity of a point on a thread or the bolt head.

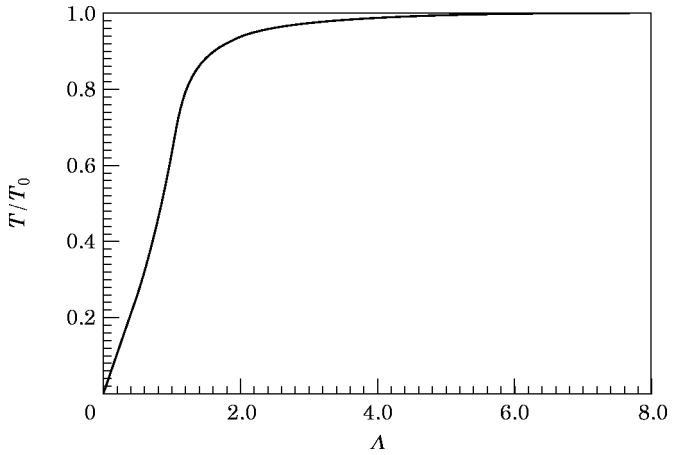

Figure 12. Relationship between the normalized friction torque T/T_0 and velocity ratio Λ.

$$\cos\alpha = (\Lambda - \sin\theta)/\sqrt{1 - 2\Lambda\sin\theta + \Lambda^2}. \tag{38}$$

q is defined as the normal force per unit area. Therefore, the friction force per unit area is μq. If there is no transverse motion of the ring of Figure 11, then the friction torque T_0 which resists loosening is due to the friction forces over the whole ring:

$$T_0 = \int_A (\mu q r)\,\mathrm{d}A. \tag{39}$$

On the other hand, if the ring is moving as shown in Figure 11, then according to the principle discussed previously, the friction torque T becomes

$$T = \int_A (\mu q r\cos\alpha)\,\mathrm{d}A = \int_A (\mu q r)\,[(\Lambda - \sin\theta)/\sqrt{1 - 2\Lambda\sin\theta + \Lambda^2}]\,\mathrm{d}A. \tag{40}$$

This function can be evaluated for fixed values of Λ. Figure 12 shows the relationship between T (normalized by the zero motion friction torque T_0) and Λ.

From Figure 12, it can be seen that if Λ approaches zero with $|\mathbf{v}_t| \neq 0$, then T approaches zero since T_0 does not vary with Λ. In this case, the threads or bolt head are free of the resisting torque and any small off-torque, such as the torque resulting from the lead angle, may turn the bolt. The amount of this turning, however, will be small since $|\mathbf{v}_c|$ is no longer equal to zero once the bolt turns and T may increase rapidly to the value where the off-torque is not large enough to overcome the effective friction torque. Then the bolt quits loosening.

6. CAUSES OF DYNAMIC BOLT SELF-LOOSENING

Due to the effect of the lead angle, an internal off-torque T_{off} is created under the application of the preload Q. This off-torque wants to rotate the bolt in the loosening direction and its value is equal to [5]:

$$T_{off} = Q r_e \tan\psi, \tag{41}$$

where r_e is the equivalent friction radius of the thread and ψ is the lead angle. Due to the friction on the threads, there exists a torque T_t resisting rotation of the bolt [18]:

$$T_t = Q\mu_3 r_e / \cos \phi, \tag{42}$$

where ϕ is the thread angle and μ_3 is the coefficient of friction at the threads. There also exists a resisting torque T_h on the bolt head:

$$T_h = Q\mu_2 r_{eh}, \tag{43}$$

where μ_2 is the coefficient of friction at the bolt head and r_{eh} is the equivalent friction radius of the bolt head. The values used for all of these variables in the simulations presented in section 7 are listed in Table 4.

If the bolt intends to rotate, it has to overcome the resistance of T_t and T_h. Generally, the value of T_{off} from equation (41) is smaller than either T_t (equation (42)) or T_h (equation (43)), so that the bolt does not spontaneously loosen. From Figure 12, if relative transverse motion (slip) occurs at the threads or at the bolt head, then the effective values of T_t or T_h, respectively, may fall below the value of T_{off}. It is obvious, therefore, that either slip at the threads or slip at the bolt head is a necessary condition, though not a sufficient condition, for bolt self-loosening to occur. For the sum of the effective values of T_t and T_h to be less than T_{off}, slip must occur simultaneously at the threads and the bolt head. Therefore, it is necessary to determine the conditions that lead to the simultaneous occurrence of slip at the threads and the bolt head.

Static experiments [9, 10] have verified that as the mass slips that no slip occurs at the threads until the mass contacts the bolt, and that no slip occurs between the bolt head and the mass if the mass contacts the bolt very slowly. In short, impact is the only

TABLE 4

Parameter values for the self-loosening simulations

Symbol	Definition	Value
r_e	Equivalent friction radius of threads (mm)	2·874
r_{eh}	Equivalent friction radius of bolt head (mm)	4·201
r_{pitch}	Pitch radius of thread (mm)	2·725
ψ	Thread lead angle (°)	4·18
ϕ	Thread angle (°)	30·0
μ_{s1}	Static coefficient of friction at plate	0·200
μ_{k1}	Dynamic coefficient of friction at plate	0·200
μ_{s2}	Static coefficient of friction at head	0·200
μ_{k2}	Dynamic coefficient of friction at head	0·200
μ_3	Coefficient of friction at threads	0·200
L	Active length of bolt (mm)	29·439
L_1	Active threaded length of bolt (mm)	14·605
L_2	Active length of bolt inside plate (mm)	9·144
I_m	Mass moment of inertia of bolt (kg m^2)	1·132E-8
m_b	Mass of bolt (kg)	9·991E-3
m_d	Mass of disk (kg)	9·991
k_1	Hertz contact stiffness (N/m)	9·282E8
k_2	Bending stiffness of bolt (N/m)	1·490E6
k_L	Axial stiffness of bolt (N/m)	2·452E8
β	Damping to stiffness constant ratio (s)	1·721E-6
E	Clearance between bolt shank and hole (mm)	0·0838
A_d	Excitation displacement amplitude (mm)	3·556
Ω	Excitation frequency (rad/s)	64·72

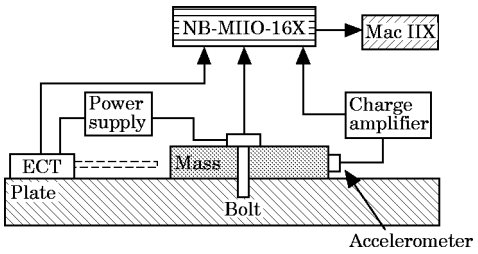

Figure 13. The experimental setup for dynamic tests.

phenomenon which can cause simultaneous slip at the threads and the bolt head. This implies that impact is a necessary condition for dynamic self-loosening of bolts.

To test this theory two experiments were run with the apparatus depicted in Figure 13. The plate was mounted on a shaker table which was subjected to a harmonic transverse displacement. An accelerometer, an eddy current transducer (ECT), and an instrumented bolt were used to measure the absolute acceleration of the mass, the relative displacement between the mass and plate, and the preload in the bolt, respectively.

At first the shaker table was run at a fixed displacement amplitude while the harmonic excitation frequency was increased. Three sets of data (from the ECT, the accelerometer, and the instrumented bolt) were acquired at low sampling rates. As the frequency was increased the acceleration amplitude also increased, until the acceleration excitation was large enough to cause motion to occur between the mass and the plate (as monitored by the ECT and the accelerometer). The experiment was stopped when Q_m (the measured preload) went to zero, signalling the total failure of the bolted connection. Results from this test are shown in Figure 14. For the system described in this paper, the threshold frequency was found to be 10·3 Hz for an initial preload $Q(0)$ of 267 N.

For comparison a second test was run with the same conditions as in the first test, but at a fixed frequency (9·85 Hz), which was selected to be just below the threshold frequency at which impacts occurred. This threshold frequency is determined based on the values of the clamping force Q, the excitation displacement amplitude A_d, the mass m_d, and the coefficient of friction μ_{s1}. This test lasted for 10 h (354 600 cycles of the excitation motion) and no dynamic loosening took place (Figure 15). These results strongly support the theory that impacts play a critical role in bolt self-loosening.

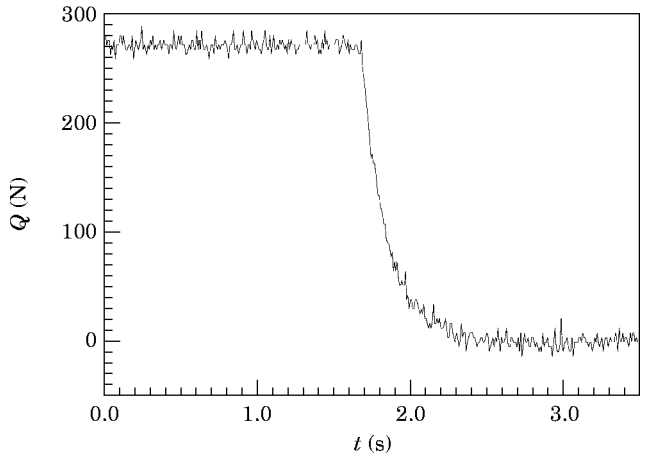

Figure 14. Time history of the preload as the excitation frequency is increased.

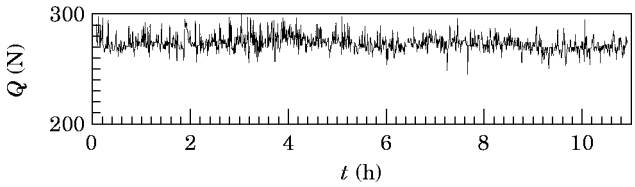

Figure 15. Time history of the preload for a fixed excitation frequency.

An analysis of the entire dynamic bolt self-loosening process as modelled above discloses that the relative motion between the bolt head and the clamped mass is a more significant phenomenon than is the transverse motion between the male and female threads. This is true because the friction radius is larger at the bolt head than at the threads, and consequently the friction torque that must be overcome by the off-torque is larger at the bolt head. Additionally, the amplitude of the relative motion is smaller at the bolt head, because the Hertz contact stiffness k_1 is significantly larger than bending stiffness k_2.

7. PREDICTION OF THE PROCESS OF BOLT SELF-LOOSENING

Consider the model of Figure 1 once again. If the excitation (amplitude or frequency) is increased, impact may occur between the bolt shank and the mass. While an impact force larger than the critical force F_{cr} (see references [9, 10]) is forcing the threads to slide transversely, the mass may slide underneath the bolt head as the mass is rebounded by the bolt shank, according to the model of Figure 5. These simultaneous relative motions make it possible for the sum of T_t and T_h, representing the resisting torques on the threads and on the bolt head, respectively, to be less than the off-torque T_{off}. Therefore, the bolt can rotate and loosen.

The angular motion of the bolt is governed by the equation

$$T_{off} - T_t - T_h = I_m \ddot{\theta}, \tag{44}$$

where I_m is the mass moment of inertia of the bolt and $\ddot{\theta}$ is the angular acceleration of the bolt. After a small time step Δ_t, the angular velocity changes from $\dot{\theta}_0$ to $\dot{\theta}$, and the angular displacement changes from θ_0 to θ:

$$\dot{\theta} = \left[\frac{(T_{off} - T_t - T_h)}{I_m}\right]\Delta t + \dot{\theta}_0, \qquad \theta = \left[\frac{(T_{off} - T_t - T_h)}{2I_m}\right](\Delta t)^2 + \dot{\theta}_0\,\Delta t + \theta_0. \tag{45, 46}$$

Here it is assumed that the torques T_{off}, T_t and T_h remain constant over the timestep Δt.

The change in the angular position $\Delta\theta$ represented in equation (46) leads to a reduction in the preload ΔQ due to the reduction in the stretch of the bolt after the bolt has rotated. The reduction in the preload is found to be

$$\Delta Q = k_L\,\Delta\theta r_{pitch} \tan(\psi), \tag{47}$$

where k_L is the axial stiffness of the bolt between the head and the threads, r_{pitch} is the pitch radius of the threads, ψ is the thread lead angle (see Table 4 for values used in this work) and

$$\Delta\theta = \theta - \theta_0. \tag{48}$$

Once the bolt starts to rotate the circumferential velocity $|\mathbf{v}_c|$ is no longer zero, and neither are T_t and T_h, which can be obtained by using equation (40) (see Figure 12). Instead, when T_t and T_h are increased to an extent such that $\dot{\theta}$ in equation (45) becomes zero, the bolt sticks again, and $|\mathbf{v}_c|$ goes back to zero. Yet, if the relative transverse velocity $|\mathbf{v}_t|$ has not vanished, implying that the impact has not ended, T_t and T_h may approach zero once again. As a result, the bolt begins to rotate again. This process repeats many times until the mass completely separates from the bolt at the end of the impact event.

The circumferential to transverse velocity ratios at the threads Λ_t and at the bolt head Λ_h are related to the relative velocities $\dot{z}$ and $\dot{z}_1$ from section 3 (see equations (27)) and the angular velocity $\dot{\theta}$ of equation (45):

$$\Lambda_t = \left| r_e \dot{\theta} \Big/ \left(\frac{L_2(\dot{z} - \dot{z}_1)}{[L_1 - L_2]} \right) \right| \tag{49}$$

and

$$\Lambda_h = |r_{eh} \dot{\theta}/(\dot{z}_1)|. \tag{50}$$

These values, along with the nominal friction torque values T_{t0} (equation (42)) and T_{h0} (equation (43)) and the Λ versus T/T_0 relationship of Figure 12 can be used to determine the values of T_t and T_h needed in equations (45) and (46).

Combining the motion model of equations (27) with the self-loosening model presented in the current section leads to a numerical simulation of the self-loosening process. Figure 16 shows the results of such a simulation (thin line with $\times$ symbol), using the values listed in Table 4, in comparison with the experimental results previously presented in Figure 14 (thick line without symbol). Note that the time axis for the experimental data in Figure 16 has been shifted from that of Figure 14 so that the apparent start of the self-loosening process corresponds with $t = 0$. Additionally, the start of the simulations results have been shifted to show the best agreement with the experimental data. The vertical dotted lines mark the periods of the harmonic motion of the shaker table. The agreement between the numerical simulation and the experimental data displayed in Figure 16 is remarkable.

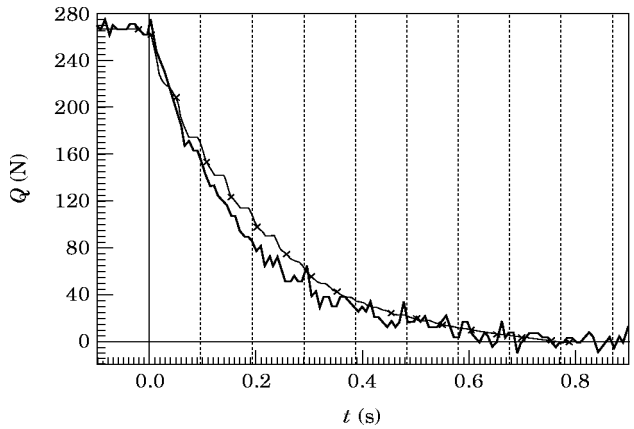

Figure 16. Comparison of simulation and experimental results of the self-loosening process. –×–, simulated results; ——, experimental results from Figure 14.

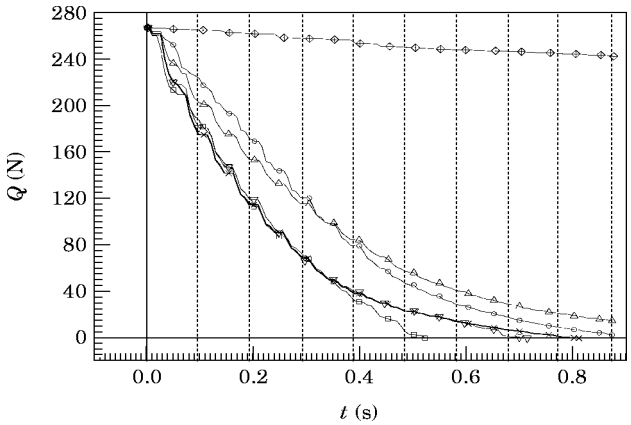

Figure 17. Self-loosening parameter study results: ×, repeated from Figure 16; ▽, $\beta = 1{\cdot}7207 \times 10^{-9}$ s; ⊕, $\mu_{S2} = 0{\cdot}22$; □, $k_2 = 14{\cdot}00 \times 10^6$ N/m: △, $k_L = 1{\cdot}618 \times 10^8$ N/m; ○, $f_{cr} = 0{\cdot}22013$.

8. DISCUSSION OF RESULTS

Before proceeding it is necessary to qualify the results presented in Figure 16. While the agreement between the simulation and the experiment is exceptional, this agreement is only reached after adjusting some of the parameter values to those listed in Table 4. In particular, it is necessary to change the values of three of these parameters (μ_{s2}, k_2 and k_L) from the values that are determined from analytical models. Additionally, the discontinuous contact damping model of equation (22) has been used and the affect of the critical force F_{cr} at the threads (see references [9, 10]) is not accounted for in the results of Figure 16. Figure 17 shows a comparison between the simulation results previously presented in Figure 16 and the simulation results for the parameter variations listed.

To quantify the affects of the discontinuous contact damping model of equation (22) the value of β (the damping to stiffness proportionality constant) was reduced by three orders of magnitude. This assured that the value of the Hertz contact damping force $c_1 \dot{z}_1$ would always be less than 1% of the sums of the absolute values of the other terms in the equations of motion (27). From Figure 17 it can be seen that this change has only a minor effect on the self-loosening process. In future studies, the more accurate model of equation (21) will be used.

Using a simple inclined plane test it is determined that the static coefficient of friction μ_{s1} between the plate and the mass is 0·22. From Table 4, it can be seen that a value of 0·20 (which is equal to the dynamic coefficient of friction μ_{k1}) is used in the numerical simulation of Figure 16. Changing this value to 0·22 barely affects the self-loosening prediction; therefore, for convenience, $\mu_{s1} = 0{\cdot}20$ is used in all of the subsequent parameter studies.

Since $\mu_{s1} = 0{\cdot}22$, it would be reasonable to assume that the static coefficient of friction μ_{s2} between the bolt head and the mass would have the same value. However, when this value is entered into the numerical simulation the results show very poor agreement with the experimental data (see Figure 17). Increasing the value of μ_{s2} increases the amount of time between the beginning and end of a stick event between the bolt head and the mass because it takes a larger force to overcome the larger friction force. This decreases the amount of time during an impact where there is relative motion between the threads and between the bolt head and mass, thereby slowing the self-loosening process, as shown in Figure 17. Since the experimental data shows a more rapid self-loosening process, a value of $\mu_{s2} = 0{\cdot}20$ is used in subsequent parameter studies. This value might be justified by

reconsidering the behavior at the bolt head to mass interface during an impact. During an impact, not only does the bolt head slide relative to the mass (as depicted in Figure 5) but it also rotates relative to the mass (see section 7). Therefore, it is quite likely that the bolt head is never totally at rest with respect to the mass during an impact, and therefore it would not be necessary to account for the affect of static friction.

k_2 represents the combined affect of the bending stiffness of the bolt and the stiffness of the threads to transverse motion. To arrive at a value for this parameter a model similar to that of Figure 6 has been developed. In this situation, however, the fixed end is replaced by the transverse resistance of the threads, which is modelled as a linear spring. If the force at the threads is below the critical value F_{cr} (see reference [9]), then the apparent stiffness of this spring is infinite. Using the values from Table 4 it is found that $k_2 = 14{\cdot}00 \times 10^8$ N/m in this situation. From Figure 17, it can be seen that the simulation results using this value are very similar to the results of Figure 16, until the preload Q is reduced to approximately 70 N ($t \approx 0{\cdot}35$ s). Beyond this point, the system goes to complete loosening ($Q = 0$) much more quickly for the larger value of k_2 than it does in the experimental data (Figure 16). It is not immediately clear from the analytical models why the value of k_2 should have this kind of effect on the self-loosening results. The smaller value of k_2 used in the simulation of Figure 16 can be justified by noting that it is quite possible that the value of k_2 varies with the preload Q, since the critical force F_{cr} will be reduced as Q decreases. Additionally, assuming that the value of k_2 is constant does not account for the fact that the transverse stiffness of the threads is finite for a transverse load at the threads which is greater than the critical force F_{cr}. On the other hand, the measured motion of the mass $z(t)$ is found to match experimental data better when the larger value of k_2 is used in a simulation. To account for all of these facts, a procedure could be established to vary the value of k_2, by varying the effective stiffness of the threads with the value of Q. This has been done, and the self-loosening results are found to be very similar to those presented in Figure 16. Therefore, for simplicity, since the smaller constant value of k_2 gives the best results for the self-loosening procedure it is used in the remainder of the parameter studies.

k_L represents the axial stiffness of the bolt, and from equation (47) it can be seen that this value has a profound effect on the rate of self-loosening. If the bolt is considered to be formed by a pair of cylindrical sections of varying radius (to represent the bolt shank and the threaded section), the axial stiffness is found to be $k_L = 1{\cdot}618 \times 10^8$ N/m. From Figure 17, it can be seen that this smaller value slows the predicted rate of the self-loosening procedure. If the bolt is assumed to have a continuous cross-section along its active length, then the axial stiffness is found to be $k_L = 2{\cdot}225 \times 10^8$ N/m, which is much closer to the value used in Figure 16 (see Table 4). The value of k_L used in Figure 16 can be arrived at by assuming a continuous cross-section while reducing the value of the effective length of the bolt to $L = 26{\cdot}718$ mm.

In reference [9], Zadoks and Yu state that there exists a critical force F_{cr} at the threads that has to be overcome before motion can occur at this interface. Since motion at the threads is a necessary condition for self-loosening, the simulation is developed so that loosening would not occur if the force at the threads is below F_{cr}. It is also assumed that the value of F_{cr} is directly proportional to the value of Q, since this threshold value is assumed to be due mainly to the affect of friction on the threads. Threfore, the relationship between F_{cr} and Q is

$$F_{cr} = f_{cr}\, Q, \tag{51}$$

where, from reference [9], $f_{cr} = 0{\cdot}22013$. In Figure 16, the value of f_{cr} is set to zero, which implies that there is no critical force F_{cr} to be overcome. In Figure 17, when the value

$f_{cr} = 0{\cdot}22013$ is used, it can be seen that the self-loosening rate is decreased, as would be expected. However, the results with $f_{cr} = 0$ are in much better agreement with the experimental data. It is possible, that for small enough values of Q the critical force F_{cr} is due only to friction, while it is due to friction and other effects for larger values of Q. In this case, equation (51) would not be appropriate, and it is possible that $f_{cr} = 0$ would be a close approximation of the resulting behavior.

Despite the fact that a number of parameter values need to be adjusted to improve the agreement between simulation and experiment, the results presented in Figure 16 are remarkable. These results show that the major factors affecting bolt self-loosening under transverse excitation are accounted for in the simulation model presented above. These factors include the piecewise continuous two-degree-of-freedom model of Figure 5 and equations (27); the Hertz contact model between the clamped mass and the bolt shank presented in section 2 and Figure 4, Figure 8 and Figure 9; and the model of the reduction of the friction torque during relative motion presented in section 5 and Figure 12.

9. CONCLUSION

In this work, the self-loosening behavior of a transversely loaded bolted connection was examined. Hertz contact theory was employed to find the relationship between contact deformation and contact force between two elastic bodies (mass and bolt shank) when impacts occur. A two-degree-of-freedom model of a bolt and a clamped mass was established, from which the time histories of the relative displacement and velocity between the mass and the bolt could be obtained. Then, if the excitation was known, the impact forces and durations could be evaluated. Additionally, models of the variations of the friction torques between the mass and the bolt head, and between the male and female thread forms, as functions of the relative velocities were presented. The combination of all of these models led to a simulation model which could be used to predict the complete bolt self-loosening procedure. The results from this simulation were verified through a comparison with experimental data.

Based on these analyses, the following conclusion can be drawn. If a bolt intends to rotate, it has to overcome resisting friction torques at the threads and the bolt head. The off-torque, which is only the source of self-loosening, is generally smaller in value than either of these resisting torques. Only when impacts occur, which lead to simultaneous slip between the threads and between the bolt head and the clamped mass, will the off-torque be greater than the sum of the effective friction torques. Therefore, for a bolted connection with a structure similar to that discussed in this work, impact is a necessary condition for dynamic self-loosening. Another significant conclusion is that relative motion between the bolt head and clamped part dominates the self-loosening process. This is not only due to a larger friction radius at the bolt head than at the threads, but is also due to the smaller amplitude of the relative motion between the bolt head and the clamped part. Based on these results, practical suggestions for the prevention of self-loosening can be developed.

ACKNOWLEDGMENTS

The work presented in this paper was completed with the support of the Sandia National Laboratories under contract numbers 27-6110 and AA-4022. The authors would like to extend their special thanks to Thomas Paez of Sandia for his vision which made this work a reality, to David Martinez of Sandia for his generous support of this work and to Norman Hunter of the Los Alamos National Laboratory for helping to repair the experimental apparatus.

REFERENCES

1. F. YEAPLE (editor) 1977 *Product Engineering* **48**, 37–42. Thread forms and torque systems boost reliability of bolted joints.
2. J. N. GOODIER and R. J. SWEENEY 1945 *Mechanical Engineering* **67**, 798–802. Loosening by vibration of threaded fasteners.
3. J. A. SAUER, D. C. LENNON and E. K. LYNN 1950 *Mechanical Design* **22**, 133–139. Bolts—How to prevent their loosening.
4. G. H. JUNKER 1969 *SAE Paper No* 69005. New criteria for self-loosening of fasteners under vibration.
5. T. SAKAI 1978 *Bulletin of the Japanese Society of Mechanical Engineers* **21**, 1391–1394. Investigation of bolt loosening mechanisms (second report).
6. K. KOGA 1969 *Bulletin of the Japanese Society of Mechanical Engineers* **13**, 140–149. Loosening by repeated impact of threaded fastenings.
7. K. KOGA and H. ISONO 1986 *Bulletin of the Japanese Society of Mechanical Engineers* **29**, 1004–1012. Study on self-loosening of bolted joints taking account of characteristics of impulsive friction.
8. D. P. HESS 1995 in *Vibration of Nonlinear*, *Random*, *and Time-Varying Systems*, *DE* **84-1**, 1165–1170. Vibration-induced loosening and tightening of threaded fasteners. New York: The American Society of Mechanical Engineers.
9. R. I. ZADOKS and X. YU 1993 in *Nonlinear Vibrations*, *DE* **54**, 79–88. A preliminary study of self-loosening in bolted connections. New York: The American Society of Mechanical Engineers.
10. X. XU 1994 *Ph. D. Dissertation*, *The University of New Mexico*, *Albuquerque*. An investigation of the self-loosening behavior of bolts under transverse vibration.
11. S. P. TIMOSHENKO 1934 *Theory of Elasticity*. New York: McGraw-Hill.
12. F. Y. CHUNG 1964 *Advanced Mathematics*. Shanghai: People's Education (in Chinese).
13. A. R. MILLER 1982 *FORTRAN Progamming for Scientists and Engineers*. San Francisco: Sybex.
14. K. H. HUNT and F. R. E. CROSSLEY 1975 *Journal of Applied Mechanics*, *American Society of Mechanical Engineers* **42**, 440–445. Coefficient of restitution interpreted as damping in vibroimpact.
15. S. P. TIMOSHENKO 1972 *Mechanics of Materials*. New York: Van Nostrand Reinhold.
16. K. M. CONE and R. I. ZADOKS 1995 *Journal of Sound and Vibration* **188**, 659–683. A numerical study of an impact oscillator with the addition of dry friction.
17. J. H. BICKFORD 1981 *An Introduction to the Design and Behavior of Bolted Joint*. New York: Marcel Dekker.
18. R. J. SWEENEY 1946 *Machine Design* June, 139–144. How to avoid loosening of bolts and nuts.